Tellus SERIES A DYNAMIC METEOROLOGY AND OCEANOGRAPHY
PUBLISHED BY THE INTERNATIONAL METEOROLOGICAL INSTITUTE IN STOCKHOLM

Analysis of a link between fall Arctic sea ice concentration and atmospheric patterns in the following winter

By SUSANNA HOPSCH[1]*, JUDAH COHEN[1] and KLAUS DETHLOFF[2], [1]*Atmospheric and Environmental Research, Inc., 131 Hartwell Avenue, Lexington, MA 02421, USA*; [2]*Alfred Wegener Institute for Polar Marine Research, Research Unit Potsdam, Telegrafenberg A43, D-14473 Potsdam, Germany*

(Manuscript received 25 October 2011; in final form 20 April 2012)

ABSTRACT

The impact of anomalous fall Arctic sea ice concentrations (SICs) on atmospheric patterns in the following winter is revisited by analysing results for two time periods: the most recent, satellite-era period (1979–2010) and a longer time-period (1950–2010). On the basis of September SICs for each time-period, an index was constructed which was used to identify anomalous high/low SIC years for both the original, as well as for the linearly detrended sea ice index. Identified years were then used to derive composites for the following winter's monthly atmospheric variables. Mid-troposphere geopotential height composites for winter months are in general reminiscent of the North Atlantic Oscillation pattern with high latitude maximum shifted towards the Barents Sea. Also, lower troposphere temperatures indicate the presence of cooler conditions over the continents during low SIC years. However, differences in the composite patterns are significant only for areas with limited spatial extent. While suggested pathways in previously published studies seem reasonable, our results show that these findings are not yet robust enough from a statistical significance perspective. More data (e.g. provided by longer, climate-quality reanalysis datasets) are needed before conclusions of impacts and feedbacks can be drawn with certainty.

Keywords: Arctic sea ice, atmospheric variability, climate variability

1. Introduction

The strong decline in autumn sea ice over the last decades has intensified interest in the relationship and interactions between sea ice conditions and the atmosphere (Herman and Johnson, 1978; Alexander et al., 2004; Seierstad and Bader, 2009 and a review by Budikova, 2009). Many previous studies view the interaction of sea ice and atmospheric circulation as a 'top-down' process (Liu and Curry, 2004; Deser and Teng, 2008; among others), where the atmosphere is providing forcing mechanisms for sea ice variability (i.e. motion, formation and melting, accretion of multiyear vs. seasonal ice). From this perspective, relationships have been shown to exist between atmospheric modes, for example the Arctic Oscillation (AO) and North Atlantic Oscillation (NAO), and Arctic sea ice concentration (SIC) – however, these relationships capture only parts of the variability and were found to be unable to explain the recent strong decline in Arctic SICs (e.g. Stroeve et al., 2011).

More recently, studies have also investigated the reverse interaction of how variations in sea ice impact the atmosphere (e.g. model studies by Seierstad and Bader, 2009; Petoukhov and Semenov, 2010; Orsolini et al., 2011). Part of this effort is derived from research directed towards understanding Arctic amplification, of which sea ice variability is an important part (Serreze et al., 2009; Screen and Simmonds, 2010; Serreze and Barry, 2011). Observations show that surface air temperatures over the Arctic region have increased at a greater rate in recent decades than when considering the global average (Serreze and Barry, 2011). It has been shown that this increase in surface temperatures is, in part, due to the reduction in sea ice cover (Screen and Simmonds, 2010).

In a recent paper, Francis et al. (2009) address the possibility of autumn sea ice extent influencing the atmospheric circulation in the following winter of the Northern Hemisphere. Their study suggests that ice conditions during

*Corresponding author.
email: shopsch@aer.com

Citation: Tellus A 2012, **64**, 18624, http://dx.doi.org/10.3402/tellusa.v64i0.18624

summer (and autumn) can impact large-scale atmospheric features in the following winter via modifying the stability of the lower troposphere, cloud variability and impacts on the poleward thickness gradient and thus implicitly the characteristics of the polar jet stream. However, this research was based on a very limited number of sampled events of high/low SICs. Honda et al. (2009) suggest that Arctic sea ice conditions in the fall can impact the winter climate over Eurasia. Using linearly regressed fields, they find that low sea ice conditions during fall are associated with cooler temperatures at low levels in the following winter over Eurasia. They also use model simulations to try to find pathways of the origin of this response, but concur that no conclusive solutions can be drawn. As the basic state of the atmospheric circulation is changing gradually, they suggest that atmospheric responses to future sea ice decrease might change as well. Overland and Wang (2010) relate the recent Arctic sea ice loss with a concurrent large-scale atmospheric circulation change. They found that the shift from the AO pattern towards a more meridional mode (referred to as the 'Arctic Dipole') in the last decade contributed to recent reductions in summer sea ice. In turn, the presence of more open water in the Arctic modifies the large-scale atmospheric circulation as the additional heat that was stored in the anomalous open water is released back into the atmosphere during autumn and early winter. Jaiser et al. (2012) describe possible pathways for how the autumn sea ice anomalies impact the atmospheric flow patterns on short to intra-seasonal timescales. Their study confirms that low sea ice conditions promote stronger heat release to the atmosphere over the Arctic Ocean and decreases the vertical static stability. This in turn impacts the baroclinic wave energy fluxes during the following months, potentially impacting the planetary wave patterns on seasonal timescales.

The potential relationship between Arctic sea ice and cloud cover was investigated by Schweiger et al. (2008). They employed a grid-point-by-grid-point composite analysis, which makes it impossible to analyse contributions from any advective processes (since neighbouring grid point averages may contain contributions from a different subset of years). Their study found that the overall radiative impact of the changes in cloud cover is small and does not contribute to autumn SIC anomalies. Furthermore, their study was based on European Centre for Medium-Range Forecasts reanalysis data (ERA-40) which has been shown to contain considerable biases in, for example, temperature of the low to middle troposphere over polar regions (Uppala et al., 2005; Screen and Simmonds, 2011), thus rendering Schweiger et al.'s (2008) results problematic. Nevertheless, other studies on Arctic amplification also indicate that changes in cloud cover have not contributed to the observed recent warming of Arctic regions (Serreze et al., 2009; Screen and Simmonds, 2010; Serreze and Barry, 2011).

Because the majority of previous studies are based on data using only a very limited number of years that furthermore are often restricted to large anomalies only ($>$ 1 *SD*), the reported results have often not been conclusive or robust enough for further statistical analysis. Our present study seeks to revisit modern datasets and investigating possible impacts of anomalous SICs during fall on the following winter's atmospheric conditions while increasing the sample size. Two different time periods are analysed (satellite era during which a strong trend in SICs was observed, and a longer time period that includes pre-satellite data which essentially has a negligible trend in SICs), and the number of data points used is increased to allow for a more robust assessment of the statistical significance of the obtained signals.

2. Data and methodology

The monthly SIC dataset from the Met Office Hadley Centre (Rayner et al., 2003) is used to identify the years with anomalously high and low SICs. The results presented in this paper are based mainly on the September SIC data for two different time ranges: 1979–2010 and 1950–2010. The former period reflects the most recent conditions and makes use of satellite data as well as other observational data and thus incorporates the most reliable data sources. The latter time series, which includes the earlier time range, is used for comparison, but it should be kept in mind that the associated error bars of the data for the pre-satellite era are larger. To assess the possible relationships of SIC and characteristics of the atmosphere in the months following the autumnal sea ice minima, monthly data from the NCEP–NCAR Reanalysis (NNR) (Kalnay et al., 1996) are used. Even though the NNR is not as modern as other more recent reanalysis datasets, such as Modern Era Retrospective Analysis (Rienecker et al., 2011), Climate Forecast System Reanalysis (Saha et al., 2010), ERA-interim (Dee and Uppala, 2009) and others, it carries the benefit of providing the longest continuous time series of all available reanalysis datasets and is therefore best suited for our study. Also, while there are some known problems of identifying ice-covered grid cells and their associated surface air temperature and derivatives, a study on arctic amplification by Serreze et al. (2009) has shown that there are no significant differences in the results when using identified problematic grid cells or not.

In particular, we use the September SIC data to derive the time series for a sea ice index which is defined for the region of 70°–85°N and 90°–210°E (outlined by box in Fig. 3d). This area exhibited the largest variability in September SIC during the last several decades of the

20th century, and is significantly correlated with SICs for the Arctic Ocean as will be shown later. It also ensures that the index's amplitude is as large as possible.

The index is used to find the highest and lowest 'extreme' years with values of greater than ± 0.5 *SD* of the area-averaged SICs, respectively. Those years are furthermore used in a composite analysis, which highlights the characteristic patterns of atmospheric differences between the high/low SIC years. The statistical significance of the results is assessed using a simple *z*-test (test for differences of mean under independence, i.e. a variant of a *t*-test). It tests whether the selected members of the low SIC composites are different from the high SIC members or not, even though they are chosen from the same overall population; see also Chap. 5.2.2. in Wilks, 2006).

3. Results

3.1. High and low SIC years

Figure 1 shows the 1979–2010 September SIC index as 'observed' (Fig. 1a) and the detrended and standardised sea ice index for the same time period (Fig. 1b). The bottom panel (Fig. 1c) shows the detrended and standardised SIC index for 1950–2010 for comparison. Selected years from the highest SIC subset are indicated by the red squares in the time series, and the years belonging to the lowest subset are indicated by blue triangles. Note that all the selected high/low SIC years are greater (less) than $+(-)\,0.5$ *SD* from the time series mean. Furthermore, we also increase the threshold of selected years for the longer time period and retain only the highest/lowest 10 yr. This guarantees that any obtained signals are stronger (because only more extreme years are sampled); it also provides for more data points for statistical analysis. Not surprisingly, the original (Fig. 1a) time series for 1979–2010 indicates that the highest years belong to the early part of the time series, whereas the lowest years occurred during the latter part of the period, which is reflective of the strong decline in SIC over the last two decades. Note that the distribution of high versus low SIC years is more evenly distributed when the detrended and standardised time series is taken into account (Fig. 1b). In comparison, composite figures concerning the long-time period (1950–2010) are only shown for the detrended and standardised time series (Fig. 1c; supplementary information shows results for the 1950–1978 period). This highlights the impacts of sea ice anomalies on atmospheric flow from an interannual perspective and allows results from the longer time period to be compared with the results from the modern time period.

To test the sensitivity of the area chosen for the sea ice index, we generated additional SIC indexes based on four additional regional quantifiers [(1) Arctic Ocean (ArcO, 70°–85°N, 0°–360°W), (2) Barents/Kara Sea (BarKar, 70°–85°N, 30°–90°E), (3) Chuckchi Sea (Chuck, 70°–85°N, 180°–157°W), (4) Eurasia and Barents/Kara Sea (EKB, 70°–85°N, 30°–210°E)], and computed the correlations for the time series of the various domains (see Fig. 2) with the trend included, and for the detrended series. It becomes clear that the SIC variability across the various domains is indeed dominated by the variation in the domain used in the present study – for both the original and detrended time series, see Table 1. The time series of the selected SIC index for the Eurasian area is strongly correlated with the sea ice index for the Arctic Ocean as a whole, as well as with the indexes of the subregions of the Chuckchi Sea and the larger EKB area.

To detrend the index, the linear trend was computed for the entire time series in question and this trend was then subtracted from the initial time series. The obtained time series of the index was then standardised to have zero mean and unit *SD*. For the gridded data, the linear trend was computed and subtracted from the time series for each grid point individually in order to also detrend those variables prior to computing the composite differences between the highest and lowest sea ice index years. Figure 3 shows the composite difference of September SIC between the low and high index years for the original (Fig. 3a) and detrended data (Fig. 3b) for 1979–2010 (differences are shaded, statistically significant areas of at least 95% significance are hatched). Figure 3c shows the difference map for the detrended data in the longer time period (1950–2010). As expected, the largest differences are found over the region which was used to define the SIC index. The variances for the original data of the two time periods are shown in Fig. 3d (valid for 1979–2010) and Fig. 3e (valid for 1950–2010) for comparison. Comparing the variance figures for September SICs between the two time periods highlights the strong decline in autumn SICs in the last 30 yr (indicated by the larger variance).

3.2. Composites of high and low SIC

By considering the differences between composites of atmospheric fields for high and low SIC years, possible impacts due to anomalous September SIC on these fields in the following months of Fall (September–November) and Winter (December–February) can be assessed. An example of this is shown in Fig. 4, where Fig. 4a shows the composite of geopotential height at 500 hPa using the selected low SIC years for February from the 1979–2010 period, and the composites for the high SIC years are shown in Fig. 4b. Figure 4d and e shows the same but for February from the long time series (1950–2010). The differences between low and high SIC years are shown in panels c and f, respectively, and highlight the main features that differentiate

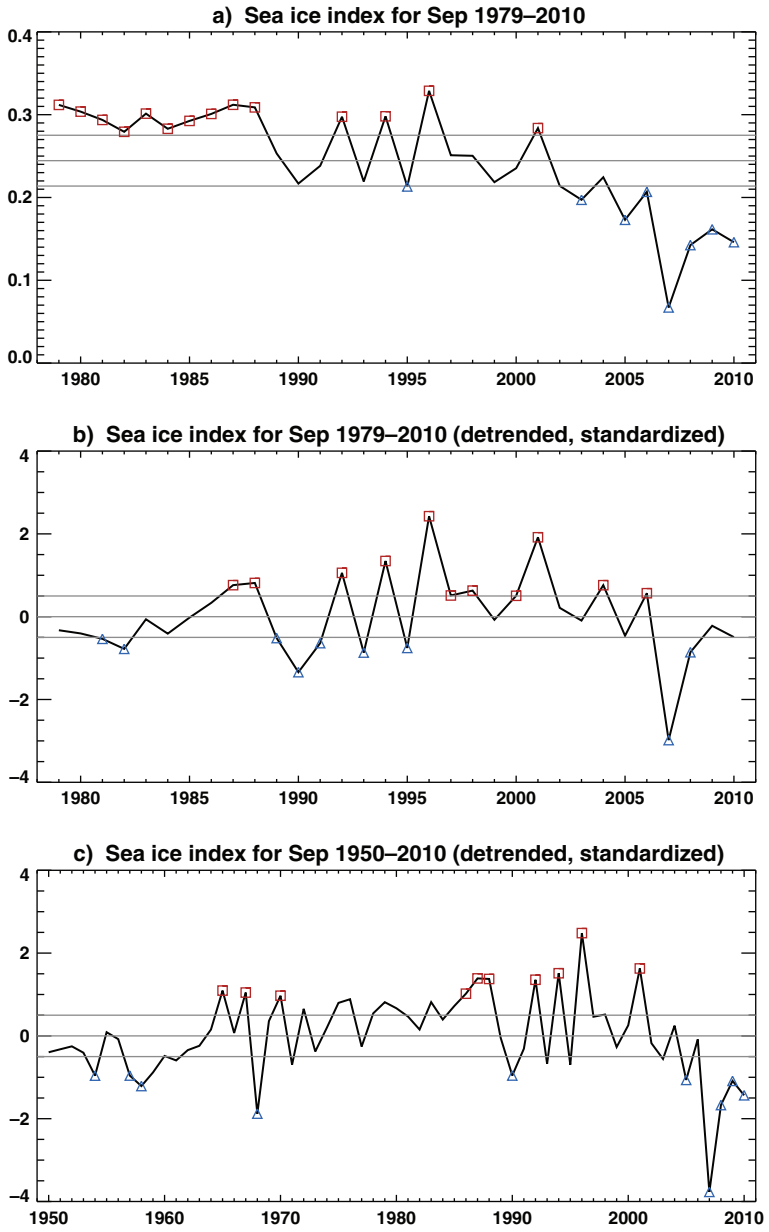

Fig. 1. Time series of 1979–2010 September SIC index (defined for region of highest variance, 70°–85°N, 90°–210°E), showing both the 'observed' index [(a) the grey lines show the time series mean and ± 0.5 *SD*), and the detrended, standardised sea ice index for the same time period (b). The bottom panel (c) shows the detrended and standardised SIC index for 1950–2010 for comparison. Selected years from the highest SIC ($+0.5$ *SD* for satellite period, top 10 yr for the long time series) subset are indicated by the red squares on the time series, and the subset belonging to the lowest years (-0.5 *SD* for satellite period, lowest 10 yr for the long time series) are indicated by blue triangles.

the two conditions from each other. Note that the atmospheric response to low and high SIC composites is not fully linear, which is why the difference between the two is useful. Furthermore by also considering composites computed from both the unmodified, original fields as well as from the detrended fields, we might also be able to obtain an additional perspective of the impacts from the observed downward trend of SIC on the Northern Hemisphere atmospheric circulation patterns and of the interannual variability.

3.3. *Impact on lower troposphere*

Figure 5 shows the difference between the lowest and highest years from 1979 to 2010 of the temperature at 1000 hPa (T1000) for the fall months of September, October and

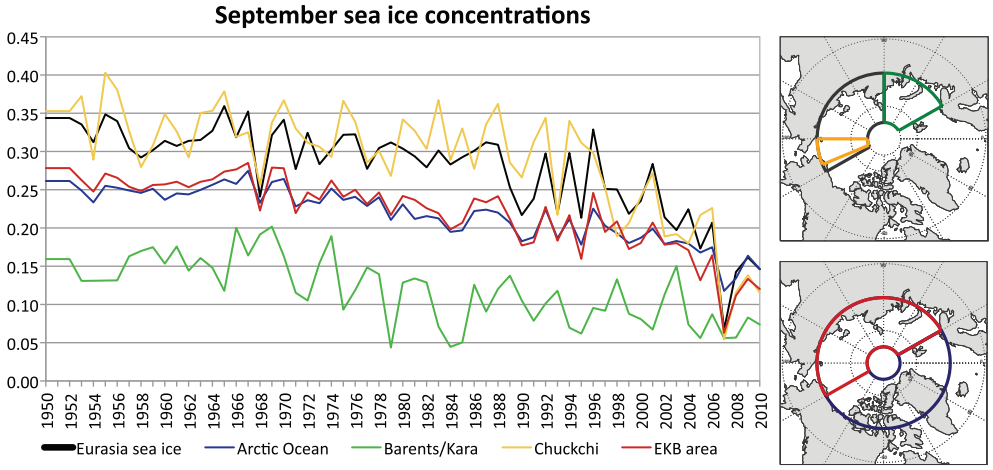

Fig. 2. Comparison of Eurasian sea ice index shown in Fig. 1 with four additional sea ice indexes, as derived for different regions for 1950–2010. The regions and their selected boundaries are: Arctic Ocean (ArcO, 70°–85°N, 0°–360°W), Barents/Kara Sea (BarKar, 70°–85°N, 30°–90°E), Chuckchi Sea (Chuck, 70°–85°N, 180°–157°W) and Eurasia and Barents/Kara Sea (EKB, 70°–85°N, 30°–210°E).

November (top to bottom) using the original NNR data (left panels, Fig. 5a–c), the detrended NNR data (middle panels, Fig. 5d–f), and of the detrended NNR data from the longer time period (1950–2010) in the rightmost panels for comparison (Fig. 5g–i). Differences are shaded according to magnitude, and statistically significant regions are contoured at the 95 and 99% significance levels. The presence of anomalous warming during low SIC years over the Arctic region is apparent in the original time series (Fig. 5a–c), and is reflective of the upward trend in lower level temperatures that has been observed over the last decades. The detrended composite difference for the modern time period (Fig. 5d–f) shows that anomalous warming is associated with low SICs over mainly the Arctic Ocean off Siberia, whereas some areas over the northernmost continents tend to be somewhat cooler in those years. Also statistically significant differences tend to decrease in space over the course of the months. The panels for the detrended fields from the longer time period (Fig. 5g–i) show the monthly variation in lower tropospheric temperature differences, confirming the anomalous warming over the Arctic Ocean off Siberia.

Figure 6 shows the same information, but for the winter months of December, January and February. The two most prominent features shown in Fig. 6a–f are the apparent temperature differences that emerge over the Arctic Ocean and continental areas for both original (Fig. 6a–c) and detrended grids (Fig. 6d–f). The maps indicate that lower tropospheric temperatures are colder over the Arctic during high SIC years than during years with low September SICs.

Table 1. Correlation coefficients between the various regions' SIC indexes for both the satellite period (1979–2010) and long period (1950–2010) time series

Correlations	With trend 1950–2010	1979–2010	Detrended 1950–2010	1979–2010
Eurasia/ArcO	*0.9284*	*0.9605*	*0.8108*	*0.8998*
Eurasia/BarKar	*0.4908*	0.2178	−0.1090	0.0880
Eurasia/Chuck	*0.9044*	*0.8808*	*0.7819*	*0.6765*
Eurasia/EKB	*0.9630*	*0.9703*	*0.9060*	*0.9249*
ArcO/BarKar	*0.7349*	*0.4049*	*0.3731*	*0.3916*
ArcO/Chuck	*0.8361*	*0.8736*	*0.5953*	*0.6681*
ArcO/EKB	*0.9805*	*0.9806*	*0.9313*	*0.9519*
BarKar/Chuck	*0.3927*	0.1597	−0.2227	−0.0151
BarKar/EKB	*0.7075*	*0.4475*	*0.3219*	*0.4600*
Chuck/EKB	*0.8549*	*0.8462*	*0.6495*	*0.5959*
Two-tail Pear cc	df = 59	df = 30		
0.05	0.2521	0.3494		
0.1	0.2126	0.2960		

Statistical significance at the 95% levels is shown in italics.

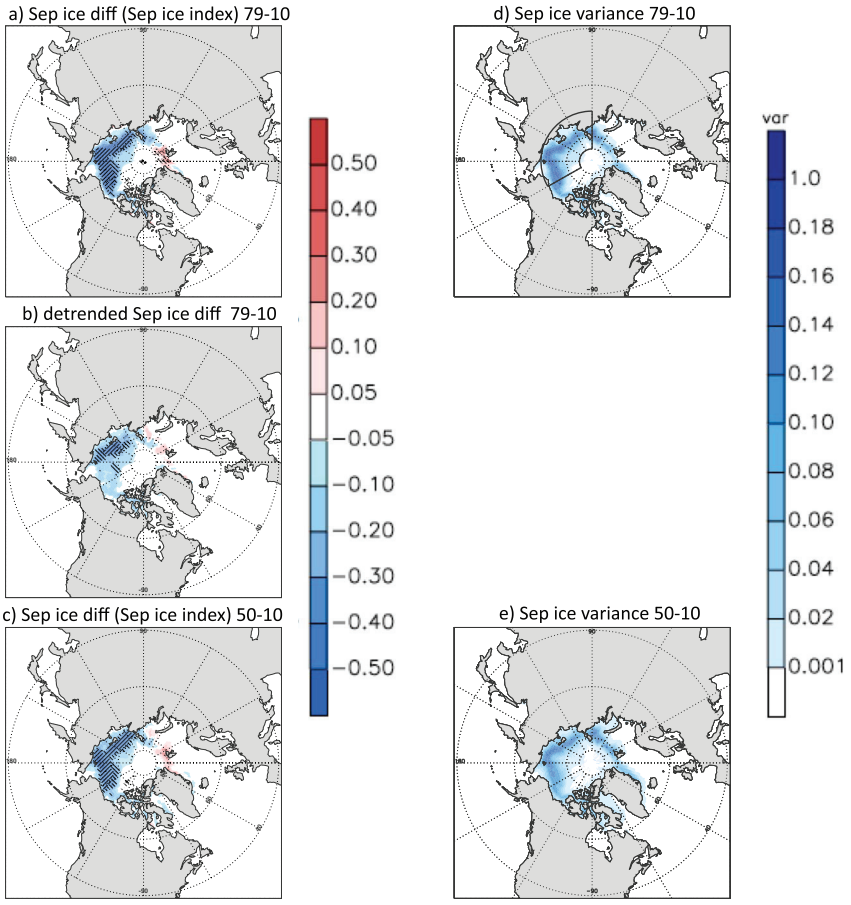

Fig. 3. September SIC difference between lowest and highest (± 0.5 *SD*) sea ice index years. The difference of the original data for 1979–2009 is shown in the top left panel (a), the difference of the composite for the detrended data for the same period is shown in (b) (middle panel). The difference of the detrended data for 1950–2009 is shown in (c) (bottom left panel) for comparison. Statistically significant regions are hatched (95% significance: back hash and 99% significance: forward hash). The variance for September sea ice from the original data for the two time periods is shown in (d) (1979–2009) and (e) (1950–2009). The box used to derive the sea ice index is outlined in (d).

This result intuitively makes sense, as heat fluxes from a more frozen Ocean surface are much smaller than from more open waters. More interesting, however, are the results obtained for the temperature differences over the continents. The panels indicate that lower troposphere temperatures during low SIC years are colder than during high SIC years. This pattern is particularly apparent in the composite differences over the Eurasian continent for December and January using the original data (Fig. 6a and c). While colder temperatures can be found around 40°–50°N in the December composite, by February the region of colder temperatures has migrated towards north, to approximately 60°–70°N. The patterns for these temperature differences in mid to late winter are only statistically significant for rather limited spatial areas.

Conceptually, the results for the detrended data (Fig. 6d–f) are similar, even though some differences exist as well. While temperatures in the original data during low SIC years were found to be coolest over the Eurasian continent, the detrended data indicates that the cooler temperatures are found over North America instead (Fig. 6d), although somewhat cooler temperatures are also found over Eurasia (same position as in original data, but differences to high SIC years are smaller in December). As before, the regions experiencing colder conditions during low SIC years appear to expand in area as winter progresses, but still only few, spatially limited areas show a statistically significant signal.

Applying the same approach to the longer time series for data from 1950 to 2010 (Fig. 6g–i) provides slightly

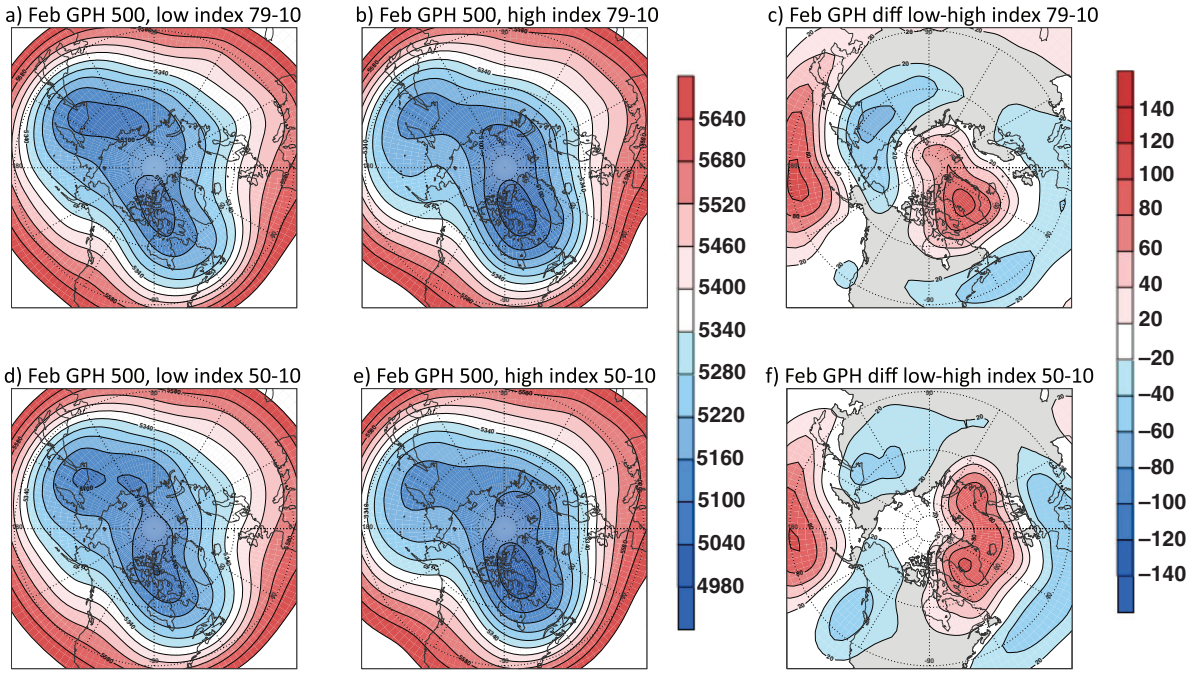

Fig. 4. Illustration of how composite differences are generated. (a) The composite of geopotential height at 500 hPa using the selected low SIC years; the composites for the high SIC years are shown in (b). The difference between panel a and panel b is shown in the panel c and highlights the main features that differentiate the two conditions from each other. (d) to (f) are same as (a) to (c) but for 1950–2010.

different patterns, where the regional 'centres of action' are now found at different locations (most notably over North America in February, Fig. 6i) for the composited months. However, the main characteristics of colder temperatures in the lower troposphere over the ocean during high SIC years and colder temperatures over the continents during low SICs still hold. The same qualitative results are obtained when the original data are used (not shown).

As expected, regional differences in the composite-difference patterns between the two time periods exist. Nevertheless, the physical pathways responsible for enabling anomalous high or low September SICs to impact the atmosphere in the following winter months should be similar between the two periods. The lack of such a clear signal, in concert with limited statistical significance only renders the findings of cooler conditions over the continents during low SIC years to be suggestive, but not certain. Nevertheless, the results seem to support recent findings by Inoue et al. (2012), where it is shown that low winter SIC years over the Barents Sea moderate the cyclone tracks there and generate a high-pressure anomaly along the Siberian coast in winter. This anomaly transports warm air to the Arctic and cold air to Siberia. The difference in cyclone tracks between high- and low-SIC years triggers what they call Warm-Arctic Cold-Siberian anomaly. During low ice years the lower baroclinicity over the Barents Sea is connected with fewer cyclones which increases the anticyclonic anomaly over the Siberian coast and a colder Eastern Hemisphere (similar to the patterns we find as shown in Fig. 6e–f and h–i).

3.4. *Impact on mid-troposphere*

Previous studies by Francis et al. (2009), Honda et al. (2009), Overland and Wang (2010) and others have noted the emergence of an NAO-like signal of the atmospheric flow during winter, where the presence of less September sea ice has been associated with a negative NAO-type pattern of the atmosphere in the following winter. To test the effect of September SIC on the free atmosphere, we therefore analyse the impact on geopotential height at 500 hPa (GPH500) for the following fall and winter months (see Figs. 7 and 8). The differences between lowest and highest years from 1979 to 2010 are shown for September to November (top to bottom, left panels) for the original data (Fig. 7a–c), the detrended data (middle panels, Fig. 7d–f) and for the detrended data from the longer time period (1950–2010) in the rightmost panels for comparison (Fig. 7g–i). Differences are shaded according to magnitude, and statistically significant regions are contoured at the 95 and 99% significance levels. The differences in mid-tropospheric geopotential heights

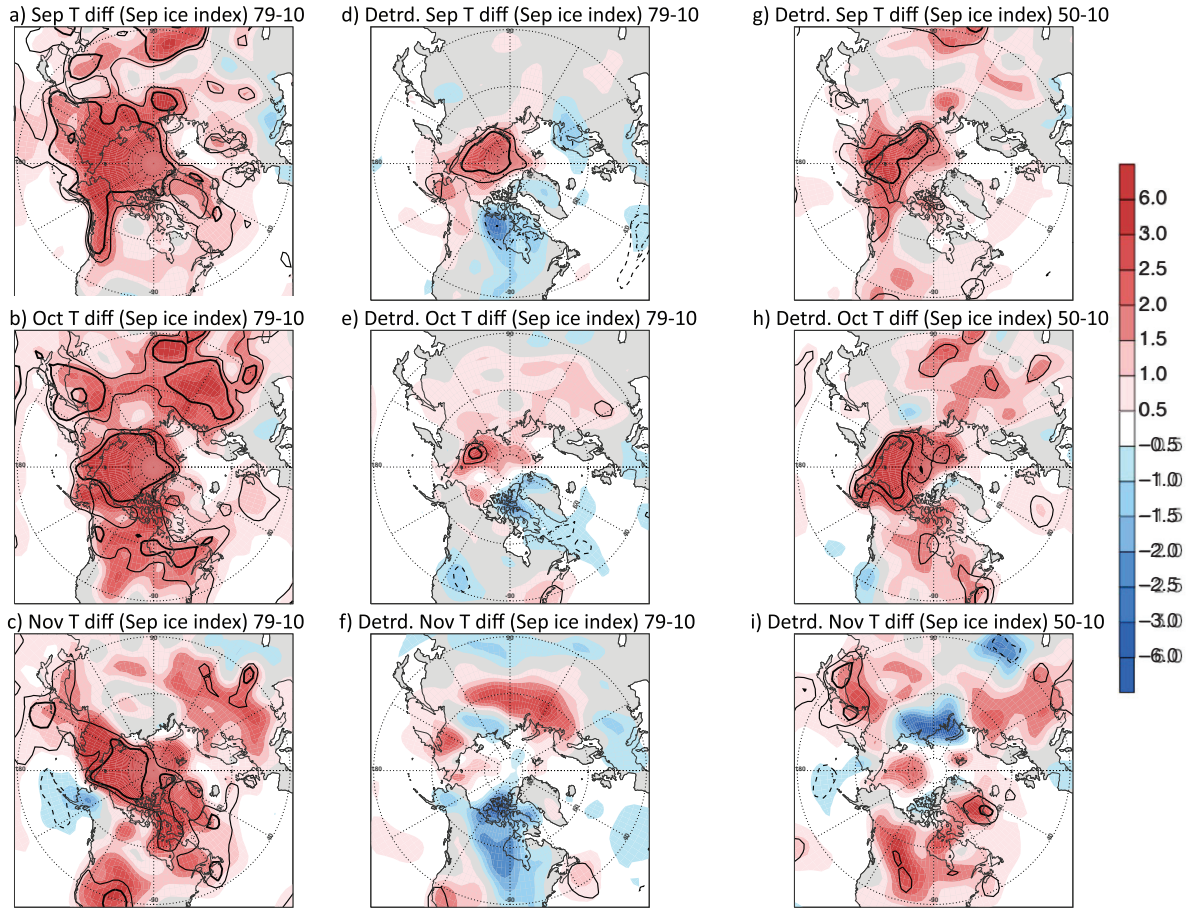

Fig. 5. Difference between lowest and highest (± 0.5 *SD*) years from 1979 to 2010 using September SIC index for region 70°–85°N, 90°–210°E of T1000 (temperature at 1000 hPa, shaded) for September, October, November (top to bottom) of NNR original data (left panels, a–c) and detrended NNR data (middle panels, d–f), and for detrended NNR data from the longer time period (1950–2010) in rightmost panels (g–i). Statistically significant areas are enclosed in black contours at the 95 and 99% significance level.

between low and high SIC years for the fall months (Fig. 7a–c) are not as clear and readily understandable as what was seen in the lower troposphere temperature differences from Fig. 5. The composite differences for the original and detrended geopotential heights in the satellite period (Fig. 7a–c and d–f, respectively) appear not to evolve in a coherent manner, and similarly when the longer time period is considered (Fig. 7g–i). However, as the months continue into winter, a clearer pattern starts to emerge.

A recent study, by Jaiser et al. (2012), shows that changes in Fall SICs can impact the large-scale atmospheric flow during winter. While their study differs from ours in that we are considering individual occurrences of discrete low fall sea ice years, whereas Jaiser et al. (2012) use two separate, but continuous time periods (and hence our designation of 'low/high sea ice years' is not identical; it is also based on ERA-interim). Nevertheless, the main features associated with anomalous low/high sea ice conditions should be comparable. Sensitivity to different reanalysis datasets should be investigated in a follow-up study, but is beyond the scope of the current study. Figure 8 is the same as Fig. 7, but shows the results for the winter months, December to February. Using the most recent time period (1979–2010), the figure confirms the presence of an NAO-type pattern for both the original and detrended data for all three months (Fig. 8a–c and d–f, respectively). Note that high SIC years are associated with lower geopotential heights in the far north over the Barents Sea and the Norwegian Sea, and slightly higher geopotential heights over southwestern Europe (December and January) and the eastern North Atlantic (February). As the months progress, the dipole pattern becomes both better defined and retrogresses westward to its more 'typical' position by February. Also, this pattern is statistically significant only for the February composite (Fig. 8c and f). The geopotential height differences for the longer time period support the hypothesis

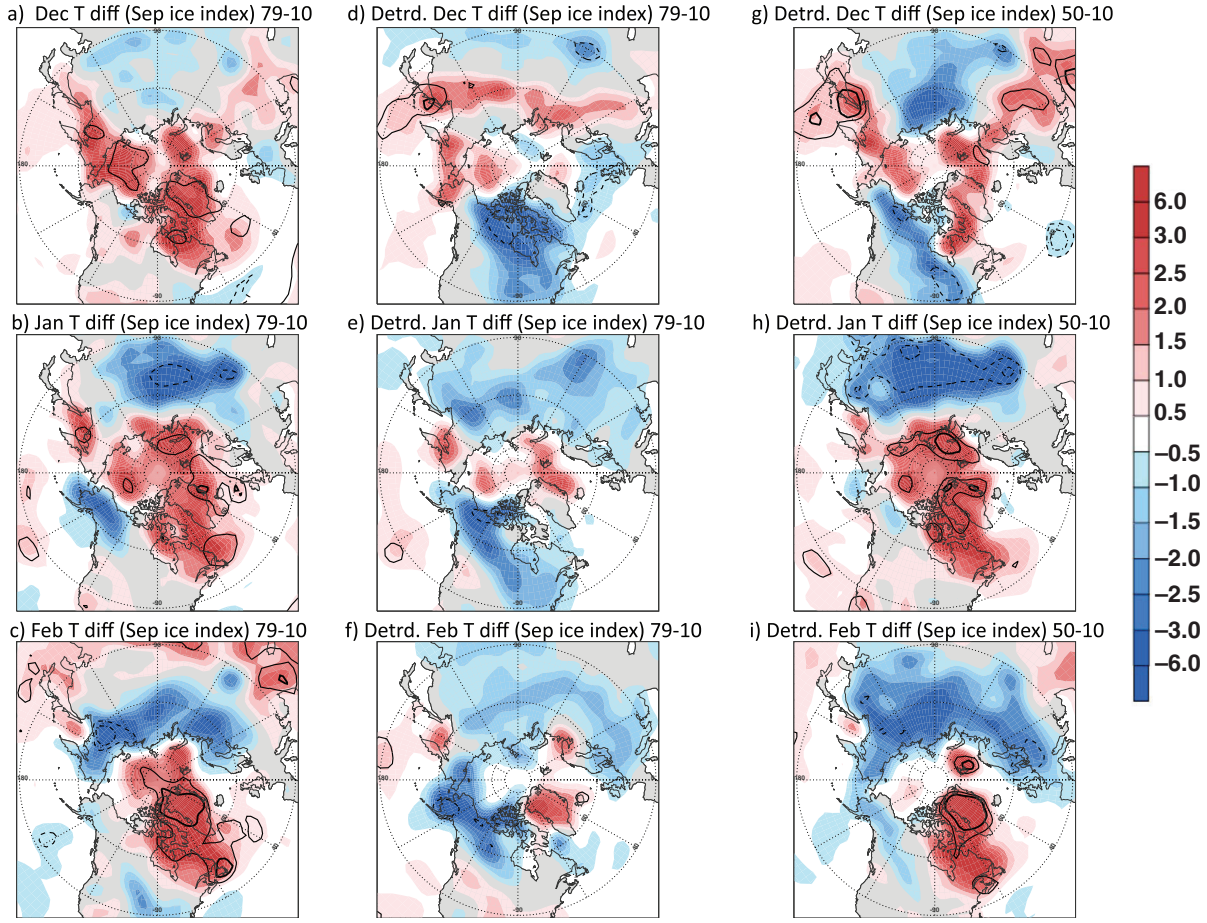

Fig. 6. Same as Fig. 5 but for difference between lowest and highest (± 0.5 *SD*) years from 1979 to 2010 using September SIC index for December, January, February (top to bottom) of NNR original data (left panels, a–c) and detrended NNR data (middle panels, d–f), and for detrended NNR data from the longer time period (1950–2010) in rightmost panels (g–i).

of lower autumn SICs forcing an NAO-type response of the atmosphere in the following winter, though most of this signal is provided for by the modern time period (cf. Fig. 6c). For completeness, the composite differences for the winter mean (December–February, DJF) are shown in Fig. 9a–c. The NAO-type pattern is apparent in the original modern time period (Fig. 9a). However, the signal is harder to interpret in the detrended data for both the modern and long time periods (Fig. 9b and c).

4. Conclusions

The strong decline in autumn sea ice over the last decades has intensified interest in the relationship and interactions between sea ice conditions and the atmosphere. Recent studies have pointed to possible impacts on atmospheric flow following anomalous SICs.

Many previous studies were based on a limited number of years and restricted to only using events with large anomalies (>1 *SD*) – a restriction that left only very few sample members for comparisons or further statistical analysis. Studies that try to identify/establish more robust signals in the relationship rely on model simulations from Global Climate Models (usually prescribing sea surface temperatures and sea ice), and thus rely inherently on the ability of these models to adequately represent the multiple processes that underlie the variability under investigation (let alone possible feedbacks).

Here we revisit the issue by analysing a longer time series and also comparing results for two different time periods: the most recent, satellite-era period (1979–2010) and a longer time series that also includes the pre-satellite period (1950–2010). A sea ice index was constructed based on September SICs for each of the two time periods. The index was then used to find the most extreme high or low SIC years (± 0.5 *SD*) for both the original sea ice data, as well as for the linearly detrended sea ice index. The identified years were then used to derive composites for the monthly

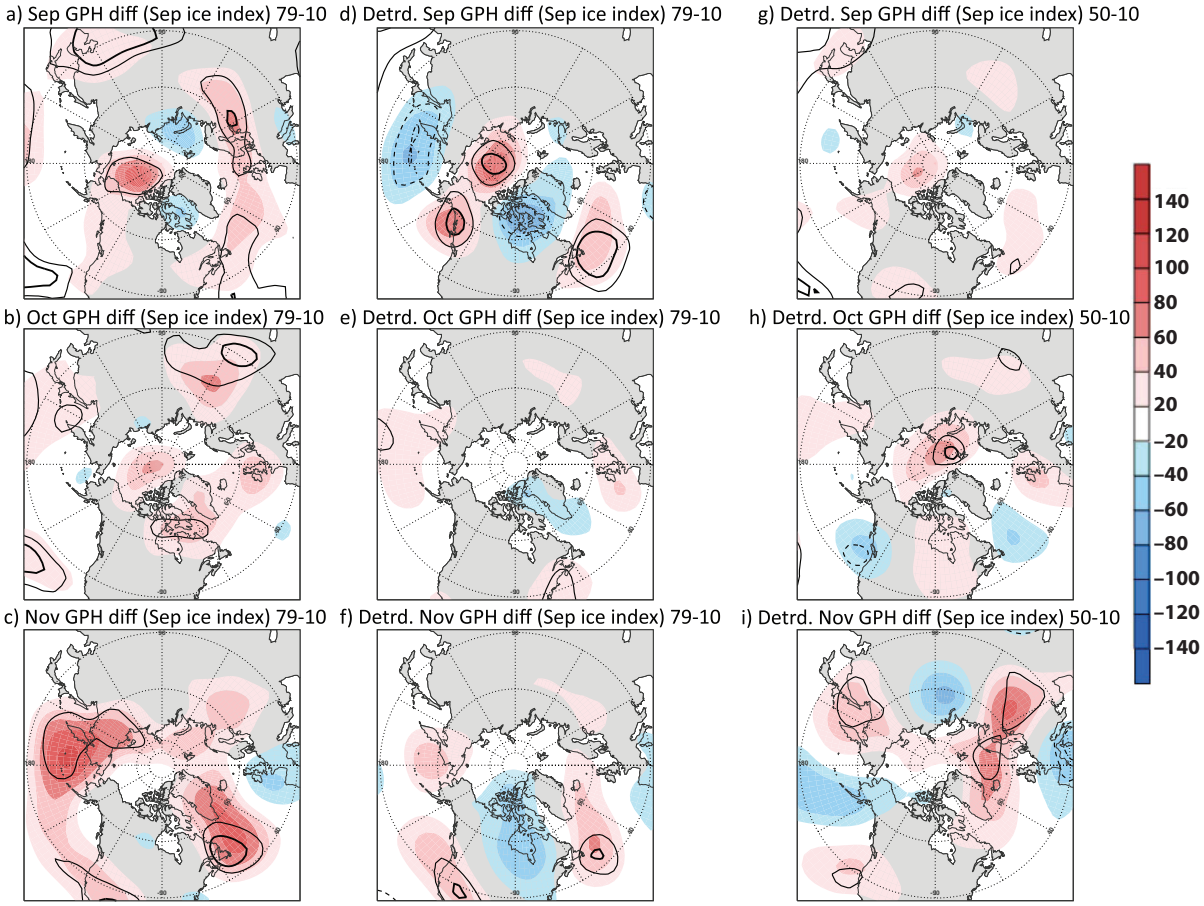

Fig. 7. Same as Fig. 5 but for geopotential height at 500 hPa (GPH 500 hPa) for September, October, November (top to bottom) of NNR original data (left panels, a–c), detrended NNR data (middle panels, d–f) and for detrended NNR data from the longer time period (1950–2010) in rightmost panels (g–i).

atmospheric variables. These gridded datasets were also used with both original, unmodified data as well as with the linearly detrended dataset, as described in Section 2.

Our study confirms the emergence of an NAO-like pattern in mid-troposphere geopotential height in the winter months following September SIC anomalies. Also, the temperatures in the lower troposphere indicate the presence of colder conditions over the continents during low SIC years. However, the differences in the composite patterns are significant only for areas with very limited spatial extent. Jaiser et al. (2012) showed on the basis of ERA interim data for the last 20 yr that Arctic heating anomalies due to low SICs in late summer trigger changes in baroclinic systems in the fall. Their study shows that the structure of large-scale planetary waves in the following winter is impacted due to an earlier onset of baroclinic instability (similar to Honda et al., 2009). The feedbacks between the mainly baroclinic response to SIC from September to November and the following barotropic response in December to February have been shown to aide the development of anomalies in Rossby wave trains over East Asia (Honda et al., 2009) and over the Pacific (Jaiser et al., 2012). As the temporal evolution of the impacts on the lower and mid-troposphere shown here suggests that the same mechanisms may be responsible, we now plan to investigate whether similar processes can be identified in our study.

While suggested pathways in previously published studies seem reasonable for the apparent signals to be ‘valid’, our results show that these results are not yet robust enough from a statistical significance perspective. Longer and reliable datasets, such as the prospective ERA-75/ERA-Clim, and other longer climate quality reanalysis datasets are needed before conclusions of the impacts and feedbacks can be drawn with higher certainty. Given the continued decrease in SIC, it will be important to continue analysing the data with the trend included, as well as with the detrended data.

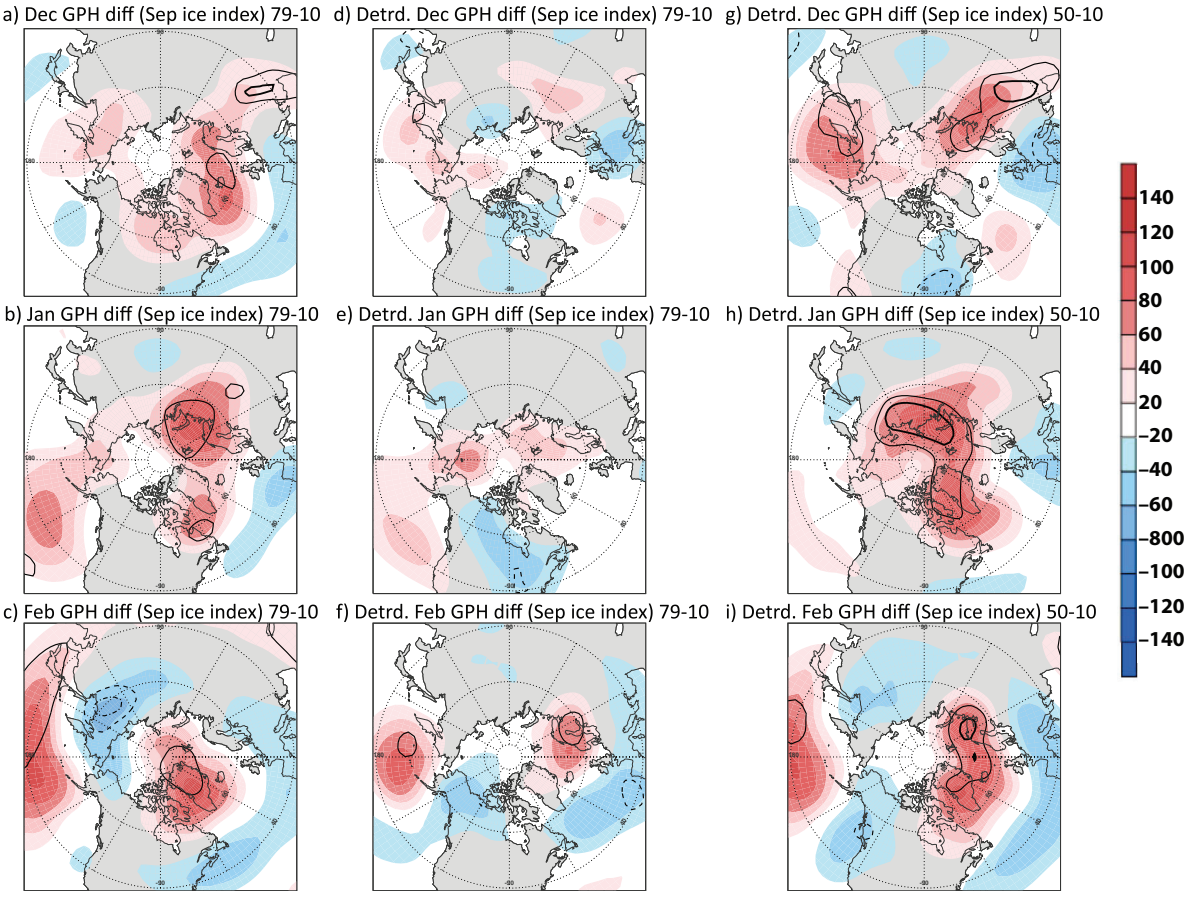

Fig. 8. Same as Fig. 7 but for geopotential height at 500 hPa (GPH 500 hPa) for December, January, February (top to bottom) of NNR original data (left panels, a–c), detrended NNR data (middle panels, d–f) and for detrended NNR data from the longer time period (1950–2010) in rightmost panels (g–i).

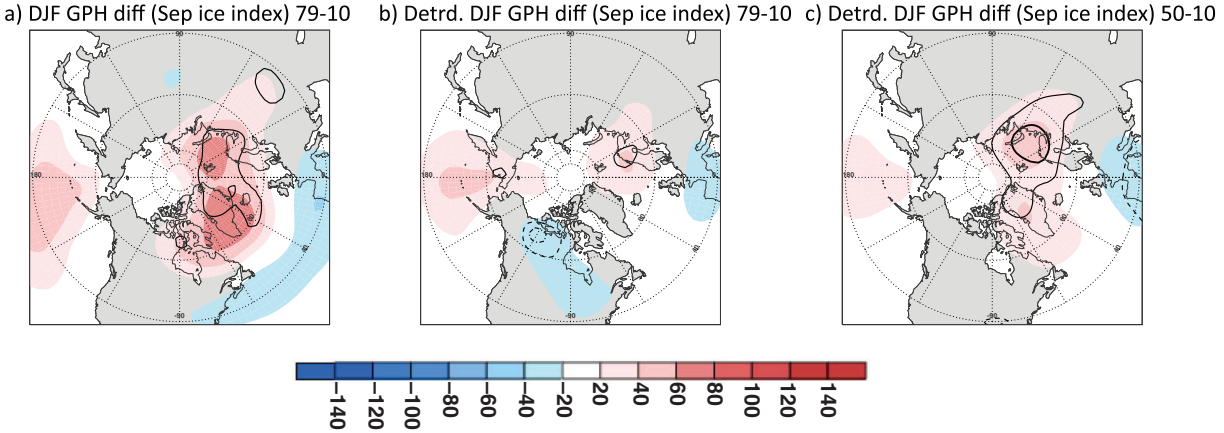

Fig. 9. Same as Fig. 8 but for geopotential height at 500 hPa, for the winter mean (December–February, DJF) of NNR original data (a), detrended NNR data (b) and for detrended NNR data from the longer time period (1950–2010, c).

5. Acknowledgements

This study was supported by grants from the National Science Foundation (ARC 0909457, ARC 0909459 and BCS-1060323). The authors would also like to thank two anonymous reviewers for their helpful comments.

References

Alexander, M. A., Bhatt, U. S., Walsh, J. E., Timlin, M. S., Miller, J. S. and co-authors. 2004. The atmospheric response to realistic Arctic sea ice anomalies in an AGCM during winter. *J. Clim.* **17**, 890–905. DOI: 10.1175/1520-0442(2004)017 <0890:TARTRA > 2.0.CO;2.

Budikova, D. 2009. Role of Arctic sea ice in global atmospheric circulation: a review. *Glob. Planet. Change* **68**, 149–163. DOI: 10.1016/j.gloplacha.2009.04.001.

Dee, D. P. and Uppala, S. 2009. Variational bias correction of satellite radiance data in the ERA-interim reanalysis. *Q. J. R. Meteorol. Soc.* **135**, 1830–1841.

Deser, C. and Teng, H. 2008. Evolution of Arctic sea ice concentration trends and the role of atmospheric circulation forcing, 1979 – 2007. *Geophys. Res. Lett.* **35**, L02504. DOI: 10.1029/2007GL032023.

Francis, J. A., Chan, W., Leathers, D. J., Miller, J. R. and Veron, D. E. 2009. Winter Northern Hemisphere weather patterns remember summer Arctic sea-ice extent. *Geophys. Res. Lett.* **36**, L07503. DOI: 10.1029/2009GL037274.

Herman, G. F. and Johnson, W. T. 1978. The sensitivity of the general circulation to Arctic sea ice boundaries: a numerical experiment. *Mon. Weather Rev.* **106**, 1649–1664. DOI: 10.1175/1520-0493(1978)106 <1649:TSOTGC > 2.0.CO;2.

Honda, M., Inoue, J. and Yamane, S. 2009. Influence of low Arctic sea-ice minima on anomalously cold Eurasian winters. *Geophys. Res. Lett.* **36**, L08707. DOI: 10.1029/2008GL037079.

Inoue, J., Hori, M. E. and Takaya, K. 2012. The role of Barents sea ice in the wintertime cyclone track and emergence of a warm-Arctic cold-Siberian anomaly. *J. Clim.* **25**, 2561–2568. DOI: http://dx.doi.org/10.1175/JCLI-D-11-00449.1

Jaiser, R., Dethloff, K., Handorf, D., Rinke, A. and Cohen, J. 2012. Planetary- and baroclinic-scale interactions between atmospheric and sea ice cover changes in the Arctic. *Tellus A* **64**, 11595. DOI: 10.3402/tellusa.v64i0.11595.

Kalnay, E., Kanamitsu, M., Kistler, R., Collins, W., Deaven, D. and co-authors. 1996. The NCEP/NCAR 40-Year Reanalysis Project. *Bull. Am. Meteorol. Soc.* **77**, 437–471. DOI: 10.1175/1520-0477(1996)077 <0437:TNYRP > 2.0.CO;2

Liu, J. P., Curry, J. A. and Hu, Y. Y. 2004. Recent Arctic sea ice variability: connections to the Arctic Oscillation and the ENSO. *Geophys. Res. Lett.* **31**, L09211.

Overland, J. E. and Wang, M. 2010. Large-scale atmospheric circulation changes are associated with the recent loss of Arctic sea ice. *Tellus*, **62A**, 1–9. DOI: 10.1111/j.1600-0870.2009.00421.x

Orsolini, Y. J., Senan, R., Benestad, R. E. and Melsom, A. 2011. Autumn atmospheric response to the 2007 low Arctic sea ice extent in coupled ocean-atmosphere hindcasts. *Clim. Dyn.* 1–12. DOI: 10.1007/s00382-011-1169-z

Petoukhov, V. and Semenov, V. A. 2010. A link between reduced Barents-Kara sea ice and cold winter extremes over northern continents, *J. Geophys. Res.* **115**, D21111. DOI: 10.1029/2009JD013568.

Rayner, N. A., Parker, D. E., Horton, E. B., Folland, C. K., Alexander, L. V. and co-authors. 2003. Global analyses of sea surface temperature, sea ice, and night marine air temperature since the late nineteenth century. *J. Geophys. Res.* **108**(D14), 4407. DOI: 10.1029/2002JD002670.

Rienecker, M. M., Suarez, M. J., Gelaro, R., Todling, R., Bacmeister, J. and co-authors. 2011. MERRA – NASA's Modern-Era Retrospective Analysis for research and applications. *J. Clim.* **24**, 3624–3648. DOI: 10.1175/JCLI-D-11-00015.1.

Saha, S. and co-authors. 2010. The NCEP Climate Forecast System Reanalysis. *Bull. Am. Meteorol. Soc.* **91**, 1015–1057. DOI: 10.1175/2010BAMS3001.1.

Schweiger, A. J., Lindsay, R. W., Vavrus, S. and Francis, J. A. 2008. Relationships between Arctic sea ice and clouds during autumn. *J. Clim.* **21**, 4799–4810.

Screen, J. A. and Simmonds, I. 2010. The central role of diminishing sea ice in recent Arctic temperature amplification. *Nature* **464**, 1334–1337. DOI: 10.1038/nature09051.

Screen, J. A. and Simmonds, I. 2011. Erroneous Arctic temperature trends in the ERA-40 reanalysis: a closer look. *J. Clim.* **24**, 2620–2627. DOI: 10.1175/2010JCLI4054.1.

Seierstad, I. A. and Bader, J. 2009. Impact of a projected future Arctic Sea Ice reduction on extratropical storminess and the NAO. *Clim. Dyn.* **33**, 937–943. DOI: 10.1007/s00382-008-0463-x.

Serreze, M. C., Barrett, A. P., Stroeve, J. C., Kindig, D. N. and Holland, M. M. 2009. The emergence of surface-based Arctic amplification. *The Cryosphere* **3**, 11–19.

Serreze, M. C. and Barry, R. G. 2011. Processes and impacts of Arctic amplification: a research synthesis. *Glob. Planet. Change*. **77**, 85–96. DOI: 10.1016/j.gloplacha.2011.03.004.

Stroeve, J. C., Maslanik, J., Serreze, M. C., Rigor, I., Meier, W. and co-authors. 2011. Sea ice response to an extreme negative phase of the Arctic Oscillation during winter 2009/2010. *Geophys. Res. Lett.* **38**, L02502. DOI: 10.1029/2010GL045662.

Uppala, S. M., KÅllberg, P. W., Simmons, A. J., Andrae, U., Bechtold, V. D. C. and co-authors. 2005. The ERA-40 reanalysis. *Q. J. R. Meteorol. Soc.* **131**, 2961–3012. DOI: 10.1256/qj.04.176.

Wilks, D. S. 2006. Statistical Methods in the Atmospheric Sciences. 2nd ed. *International Geophysics Series*. **59**, Academic Press, 627 pp.